FABRICATION, CHARACTERIZATION, AND SYSTEM-LEVEL INTEGRATION OF A Cr/Ni MEMS THERMOPILE SENSOR ON A SUB-20-µm SUSPENDED MEMBRANE FOR GAS FLOW MONITORING

NGUYEN TUAN ANH[1], HAN PHU KHANG[2], NGUYEN SI HOAI VU[1], TRAN DUY HOAI[1], NGUYEN THANH PHUONG[1], DAO MINH TUAN[1], HUYNH TRONG PHAT[1], TRUONG HUU LY[1], NGUYEN CHI CUONG[3], TRINH XUAN THANG[13]*

[1] *Research and Development Center of Hi-Tech Park (Saigon Hi-Tech Park), Viet Nam*
[2] *Faculty of Applied Sciences, Ho Chi Minh City University of Technology and Education, Viet Nam*
[3] *Faculty of Electrical Engineering Technology, Industrial University of Ho Chi Minh City, Viet Nam*
Corresponding author: thang_01038033@iuh.edu.vn
DOIs: https://www.doi.org/ 10.46242/jstiuh.v83i5.6176

Abstract. This paper presents the fabrication, characterization, and system-level integration of a Micro-Electro-Mechanical Systems (MEMS) thermopile-based gas flow sensor fabricated on a sub-20-µm suspended membrane. The device comprises a central Ti/Ni microheater and two symmetric thermopiles, each containing 20 series-connected Cr/Ni thermocouple pairs, on a 17.57 ± 1.24 µm residual silicon membrane with an approximately 1.0 µm SiO_2 isolation layer. Building on earlier membrane-thickness optimization, this study reports structural metrology, electrothermal characterization, differential flow sensing, signal conditioning, and embedded calibration of the fabricated device. Under zero-flow conditions, the upstream and downstream thermopiles exhibit closely matched Seebeck outputs. Nitrogen-flow characterization at a 5 V heater input yields single-ended cooling sensitivities of 9.83 and 8.19 µV/sccm, while an independently anti-series measurement gives a differential sensitivity of 2.21 ± 0.08 µV/sccm over 0–1100 sccm. The sensor was subsequently integrated into a standalone flow-metering prototype with signal amplification, analog-to-digital conversion, and microcontroller-based processing. A second-order polynomial was used to calibrate the nonlinear full-range response of the complete measurement chain. The prototype exhibited response and recovery times of 1.8 and 2.5 s, respectively, at 500-sccm-level. Independent validation over 0–1000 sccm produced an MAE of 27.18 sccm, an RMSE of 32.00 sccm, and a maximum full-scale error of 5.50%. Across repeated measurements, the coefficient of variation ranged from 3.87% to 8.59%. These results demonstrate a compact nitrogen-flow monitoring platform and identify ambient-temperature compensation and gas-specific calibration as priorities for further development.

Keywords. MEMS, thermopile sensor, Cr/Ni thermocouple, suspended membrane, differential measurement, flow-metering prototype, DRIE.

1 INTRODUCTION

Accurate measurement of gas flow is critical in various fields, including industrial process control, biomedical instrumentation, and automotive engineering. MEMS technology has enabled the miniaturization of thermal flow sensors, offering significant advantages over traditional macroscopic sensors, including low power consumption, high sensitivity, fast response time, and batch fabrication [1-4]. These advantages are especially important for compact flow-metering modules where the sensor must operate with limited thermal budget while maintaining adequate sensitivity and repeatability.

Among MEMS flow-sensing approaches, thermal sensors are widely used because fluid motion directly modifies the heat distribution generated by an integrated microheater. Thermal flow sensors are generally implemented in hot-wire/hot-film, calorimetric, or time-of-flight configurations [5-11]. The calorimetric configuration is attractive for low-to-moderate flow measurement because a heater is placed between upstream and downstream temperature sensors; the flow-induced temperature asymmetry can then be converted into an electrical signal. When thermopiles are used as the temperature-sensing elements, the output is generated through the Seebeck effect. It can be obtained without biasing the sensing junctions, thereby reducing self-heating and supporting stable zero-flow operation [2, 3].

The performance of a MEMS thermopile flow sensor depends strongly on thermal isolation, thermoelectric material contrast, junction quality, and the symmetry of the upstream/downstream layout. A

© 2026 Industrial University of Ho Chi Minh City

suspended membrane is commonly introduced beneath the active region to suppress heat leakage into the silicon substrate, thereby increasing the temperature gradient between the hot and cold junctions [5, 12, 13]. Recent studies have also shown that optimized thermopile geometry, heater placement, and low-thermal-conductivity support structures can improve sensitivity and extend the measurable flow range for practical gas-flow and respiration-monitoring applications. [14-16]

Metallic thermocouple pairs such as Cr/Ni remain attractive for process-oriented MEMS development because they are compatible with standard thin-film deposition, lithography, and silicon bulk micromachining. However, the relatively small Seebeck coefficient contrast of metal pairs makes the device response sensitive to fabrication variations. Therefore, reliable operation requires careful control of the released membrane thickness, the uniformity of the insulating oxide layer, the thickness and continuity of the Cr/Ni strips, and the integrity of the overlapping contact-head regions that form the thermocouple junctions.

Motivated by these requirements, this work develops and validates a Cr/Ni MEMS thermopile gas-flow sensor from microfabrication to prototype-level flow monitoring. The study first verifies the structural quality of the suspended silicon/silicon oxide membrane and Cr/Ni junctions using SEM, optical reflectometry, and surface profilometry. It then links the structural results to zero-flow electrothermal symmetry, nitrogen-flow response, anti-series differential readout, and an embedded flow-metering system based on signal amplification, ADC digitization, and polynomial calibration. This sequence establishes a complete logic chain from fabrication quality to sensor response and finally to practical gas-flow readout.

The present work builds directly on a preceding design-oriented study [17] of this Cr/Ni thermopile platform, in which experimental tests on membranes of 108.48 μm, 84.03 μm, and 42.96 μm established that reducing membrane thickness improves thermal isolation and increases output. That study identified a practical trade-off: while an ultra-thin membrane is highly desirable for enhancing thermal response, it poses significant challenges regarding electrical sensitivity, structural stability, and operational reliability during flow metering. The main advance of the present paper is therefore not a repetition of the membrane-thickness comparison, but the successful fabrication of a sub-20-μm suspended-membrane sensor followed by comprehensive structural, electrothermal, flow-sensing, and prototype-level validation.

2 SENSOR DESIGN AND WORKING PRINCIPLE

The calorimetric flow sensor operates on the principle of convective heat transfer. Figure 1 illustrates the MEMS thermopile sensor structure and layout. As shown in the cross-sectional view in Figure 1(a), the device is fabricated on a silicon substrate with a backside-etched cavity that forms a thin suspended composite membrane consisting of a residual silicon support layer and an upper silicon dioxide (SiO_2) isolation layer. A central Ti/Ni microheater and Cr/Ni thermocouple elements are patterned on the membrane.

The top-view layout in Figure 1(b) shows the thermopile arrays arranged symmetrically on the upstream (UP-TP) and downstream (DOWN-TP) sides of the microheater. The suspended sensing region has an active area of 5 × 5 mm^2. Each thermopile comprises 20 series-connected Cr/Ni thermocouple pairs. The thermocouple elements are 1000 μm long and 50 μm wide, with a 50 μm spacing between adjacent elements. The measured resistance of each thermopile is approximately 1.0 kΩ. The nearest thermopile junctions are located 500 μm from the central microheater. The Ti/Ni microheater has a length of 6000 μm and a width of 60 μm, has a total thickness of approximately 500 nm (Ti-50/Ni-450), and exhibits a measured resistance of 52.93 Ω.

At zero flow, Joule heating from the central microheater establishes a temperature gradient between the hot thermocouple junctions near the heater and the cold junctions farther away. This temperature difference generates a nonzero Seebeck voltage in each thermopile. Because the upstream and downstream thermopiles are symmetrically arranged, their temperature differences and output voltages are nearly identical under zero-flow conditions, resulting in an approximately zero differential output.

This temperature difference (ΔT) generates a differential thermoelectric voltage (ΔV), according to the Seebeck effect:

$$\Delta V = N \cdot (\alpha_A - \alpha_B) \cdot \Delta T \quad (1)$$

where, N is the number of thermocouple pairs; α_A and α_B are the Seebeck coefficients of the two thermoelectric materials.

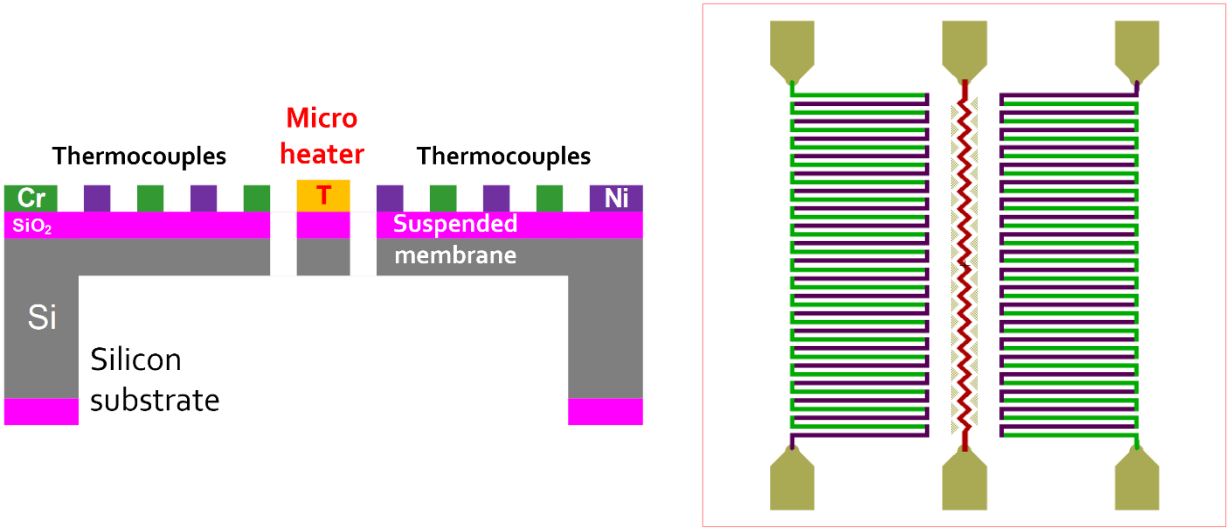
When gas flow is introduced, forced convection disturbs this symmetric temperature field. The upstream region undergoes stronger local cooling, while part of heat is transported downstream. Therefore, the temperature differences across the upstream and downstream thermopiles become unequal, producing different Seebeck voltages and a measurable differential signal.

$$\Delta V_{Up} = N \cdot (\alpha_A - \alpha_B) \cdot \Delta T_{Up} \quad (2)$$

$$\Delta V_{Down} = N \cdot (\alpha_A - \alpha_B) \cdot \Delta T_{Down} \quad (3)$$

And the differential output

$$\Delta V_{diff} = N \cdot (\alpha_A - \alpha_B) \cdot (\Delta T_{Up} - \Delta T_{Down}) \quad (4)$$



(a) (b)

Figure 1: Schematic diagram of the MEMS thermopile sensor design (a) cross-sectional overview of the structure, and (b) top-down view of the layout.

3 FABRICATION PROCESS

The MEMS thermopile sensor was fabricated on a 6-inch, (100)-oriented, 400 µm-thick, p-type silicon wafer using surface and bulk micromachining. The fabrication workflow is illustrated in Figure 2.

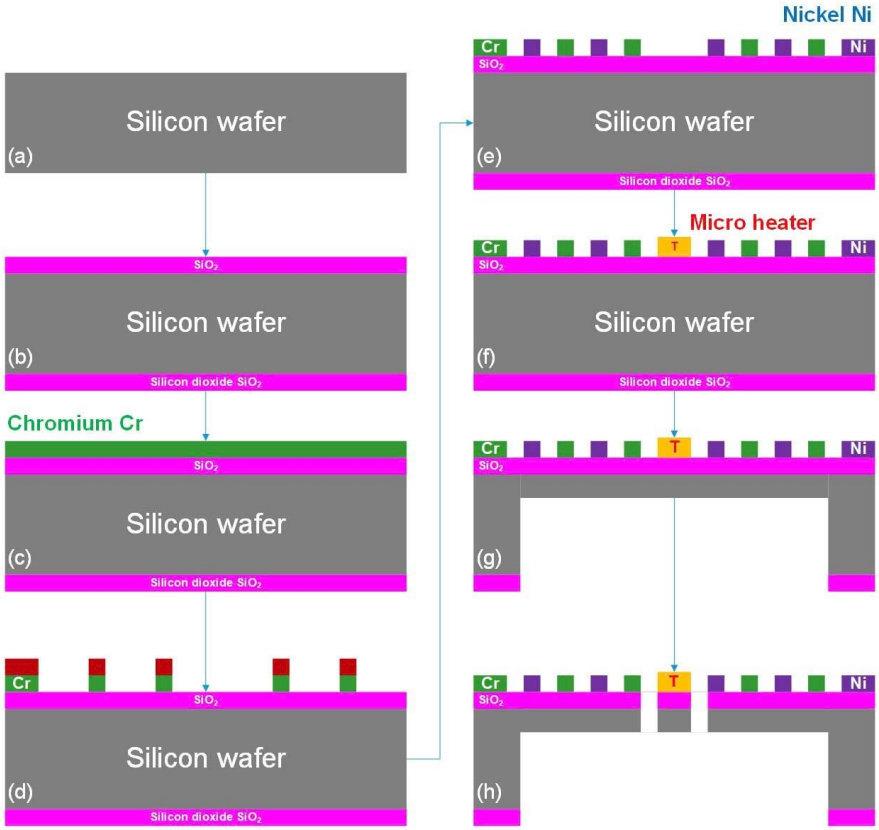


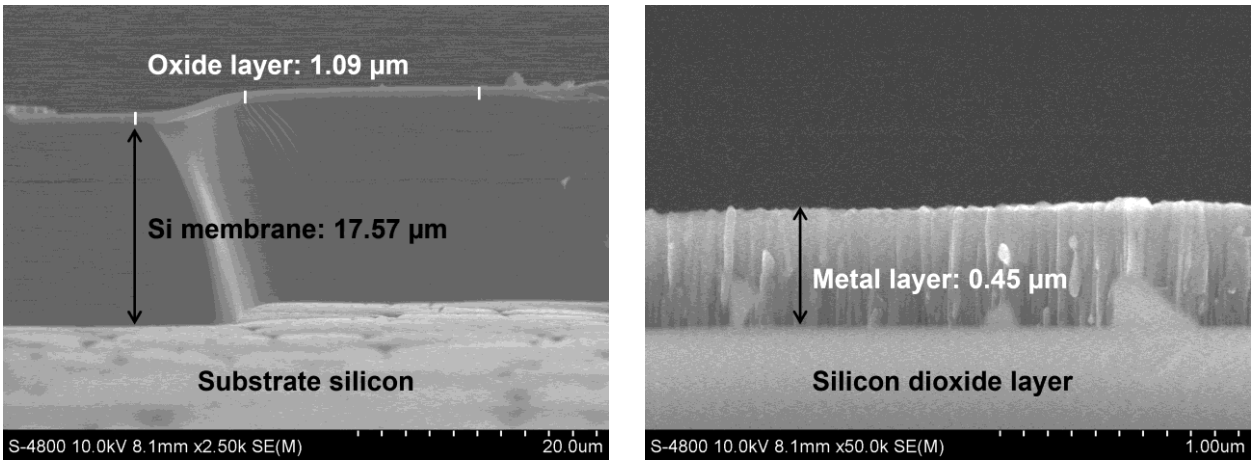
Figure 2: Schematic illustration of MEMS thermopile sensor fabrication process flow.

Initially, a 1000-nm-thick silicon dioxide (SiO_2) layer was thermally grown on both sides of the bare silicon wafer to provide front-side isolation and an oxide hard mask for backside micromachining (Figure 2(a-b)). On the front side, the metal-metal thermopile arrays were constructed. A structural chromium (Cr) layer was deposited via DC sputtering and subsequently patterned using selective wet etching (c-d). The complementary nickel (Ni) layer was then deposited by electron-beam evaporation and patterned by lift-off to form the overlapping Cr/Ni junctions and series-connected thermopile arrays, Figure 2(e). The Ti/Ni microheater and contact pads were subsequently fabricated (Figure 2(f)). The suspended membrane was released by backside DRIE of the silicon substrate through the oxide hard mask (Figure 2(g)). The reported final step was front-side RIE to define the via openings, Figure 2(h).

4 RESULTS AND DISCUSSION

4.1 Structural characterization

Cross-sectional Scanning Electron Microscopy (SEM) was used to examine the released structure and measure the layer thicknesses.

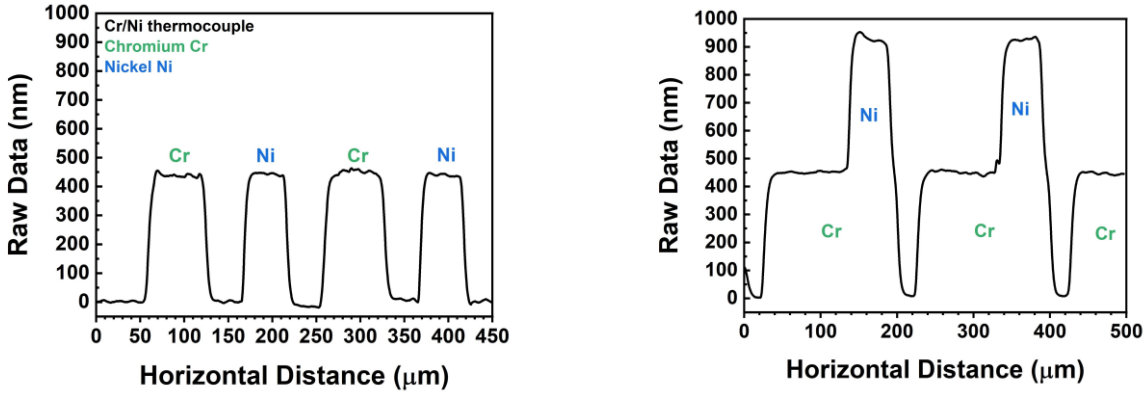


(a) (b)

Figure 3: Cross-sectional SEM images showing: (a) the silicon substrate and the details of the measured suspended membrane, including the thin silicon membrane and the oxide layer; and (b) a high-magnification view focused on the overlying metal layer on the oxide layer.

The cross-sectional SEM image in Figure 3(a) shows a residual silicon membrane of 17.57 ± 1.24 µm and an overlying SiO_2 thickness of 1.09 ± 0.13 µm. Independent optical reflectometry with a Filmetrics F40-EXR measured an average oxide thickness of 1001.39 nm, a standard deviation of 2.10 nm, and a reported nonuniformity of 0.26%. Figure 3(b) shows an overlying metal film approximately 0.45 µm thick, consistent with the nominal thickness of an individual Cr or Ni layer.

The measured layer thicknesses and distinct interfaces are consistent with the intended sensor structure at the locations examined.



(a) (b)

Figure 4: Surface profilometry measurement showing the height step of Cr/Ni pairs (a) bar-to-bar; and (b) the contact head.

Surface profilometry was used to evaluate the metal step heights (Figure 4). The isolated Cr and Ni tracks each have a thickness of approximately 450 nm. At the thermocouple contact head, the Ni layer overlaps the underlying Cr layer, producing a cumulative step height of approximately 900 nm, Figure 4(b).

4.2 Electrothermal Characterization

Electrothermal characterization was conducted in ambient air at 21–22 °C using a Suss PM5 four-probe station. A Keithley 2400 SourceMeter supplied 1-15 V DC to the central microheater in 1 V increments. The UP-TP and DOWN-TP Seebeck voltages were measured independently with a Keysight 34465A digital multimeter using a common electrical reference. The thermal performance of the Ti/Ni microheater was measured using an infrared thermometer.

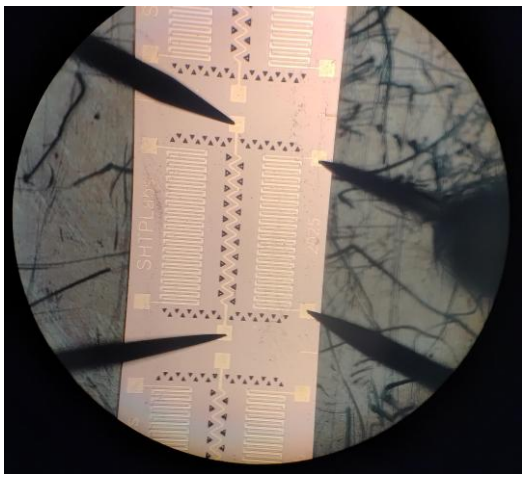
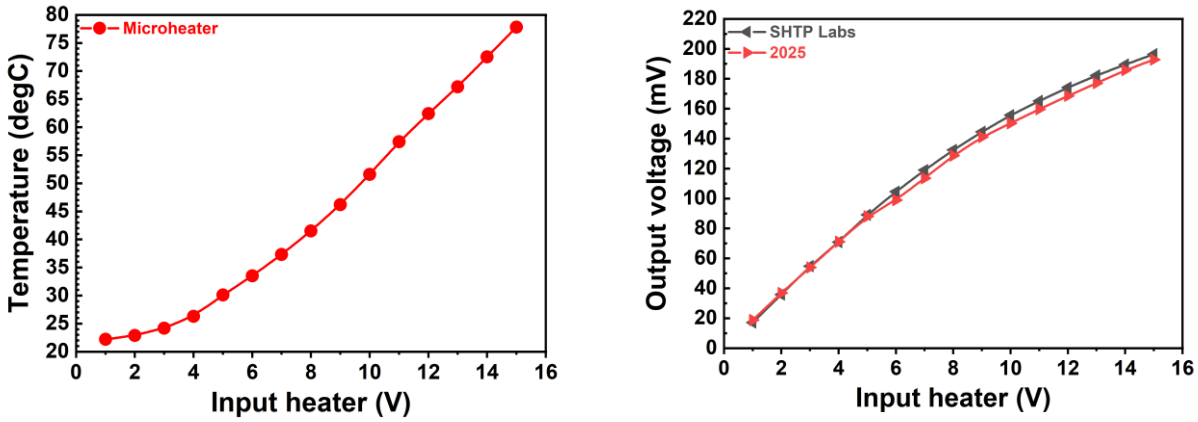


Figure 5: Top-down optical microscope image of the fabricated MEMS sensor during electro-thermal testing.

Four measurement probes are precisely positioned on the contact pads to supply the driving voltage to the central microheater and simultaneously acquire the differential output voltages from the thermopile arrays.



(a) (b)

Figure 6: Electrothermal characterization of the MEMS thermopile sensor under zero-flow conditions, illustrating (a) the measured microheater temperature and (b) the resulting thermoelectric output voltage as a function of the applied input voltage.

Figure 6 illustrates the zero-flow electrothermal response. The measured heater temperature increased nonlinearly with applied voltage, Figure 6(a), as expected from Joule heating and temperature-dependent heat loss. The upstream UP-TP and downstream DOWN-TP outputs also increased nonlinearly and remained in close agreement over the 1–15 V range (Figure 6(b)), reaching approximately 200 mV at 15 V, where the measured heater temperature was 77.8 ºC.

For comparison with the thicker-membrane devices reported in [17], the electrothermal outputs are summarized under two operating conditions. At the same heater voltage of 6 V, the devices with membrane thicknesses of 108.48, 84.03, and 42.96 µm generated output voltages of 2.03, 2.93, and 4.68 mV, respectively, whereas the present device with a 17.57 µm membrane produced 104.57 mV. This result shows that reducing the membrane thickness substantially increases the thermopile output under the same applied heater voltage.

At comparable reported heater temperatures, the previously reported 42.96 µm device generated approximately 10.8 mV at about 79 °C, whereas the present 17.57 µm sensor produced 192.74 mV at 77.8 °C under zero-flow conditions. The larger output is consistent with reduced conductive heat loss through the thinner membrane.

These results indicate that the sub-20-µm suspended membrane provides improved thermal isolation and reduces conductive heat loss to the silicon substrate, thereby increasing the temperature gradient across the thermopile junctions and enhancing the Seebeck output.

4.3 Gas flow characterization

To evaluate the dynamic response of the fabricated MEMS thermopile sensor to gaseous flow, the device was integrated into a customized gas-flow experimental system, as shown in Figure 7. Before testing, a sensor *die* was mounted and wire-bonded onto a custom printed circuit board (PCB) to establish robust electrical connections. The PCB assembly was then sealed within a specially designed flow channel to direct the gas uniformly over the suspended sensing membrane. The packaged sensor was installed in a gas flow channel with 5-mm in both width and height, corresponding to a cross-sectional area of 25 mm². High-purity nitrogen (N_2 4N) was used as the test gas.

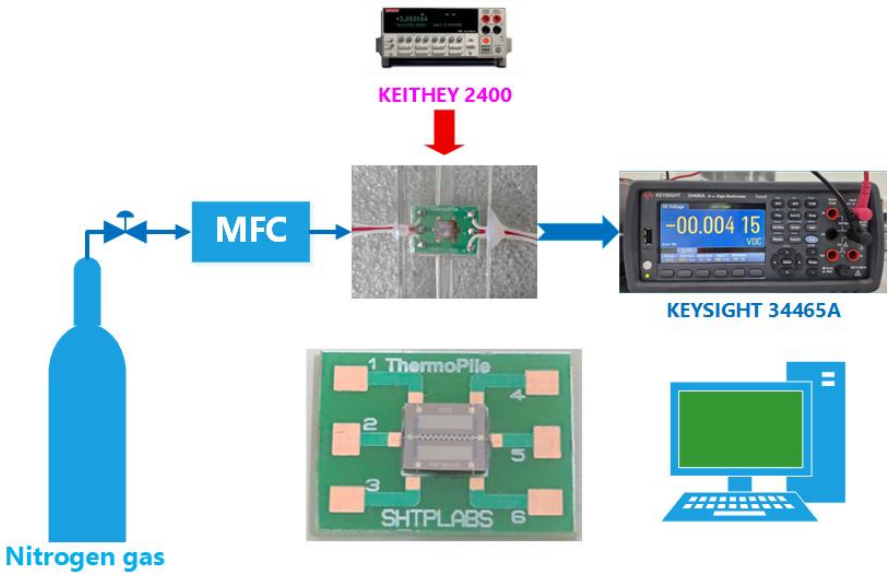
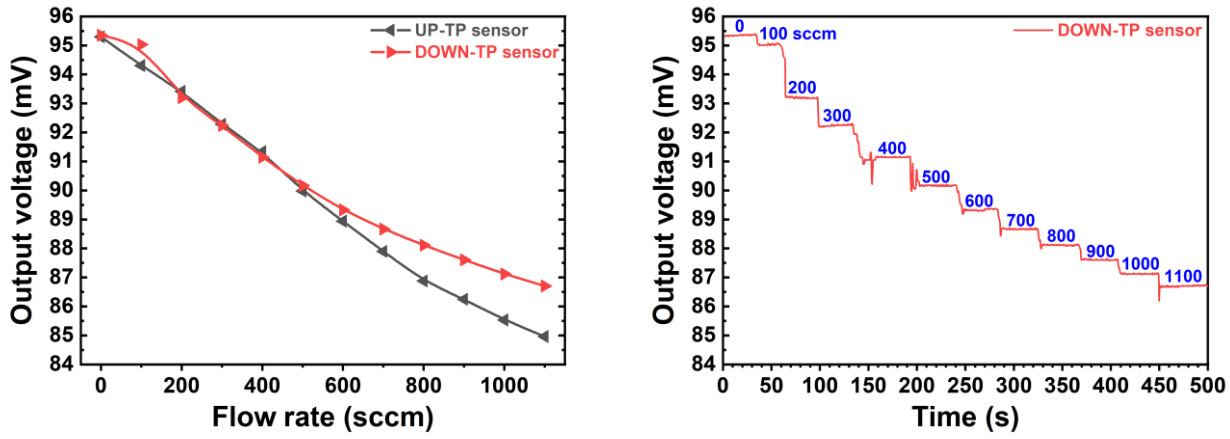


Figure 7: Schematic diagram of the experimental setup for gas flow characterization.

The gas flow was sourced from a pressurized cylinder and precisely regulated using a commercial Mass Flow Controller MFC (KOFLOC 8700 Kyoto). The Keithley 2400 maintained a constant heater voltage. The single-ended UP-TP and DOWN-TP voltages were monitored with a Keysight 34465A multimeter and logged to a computer for visualization and analysis.



(a) (b)

Figure 8: Flow measurement characteristics at a 5 V heater input. (a) Static output voltage versus flow

rate (0–1100 sccm) for both upstream and downstream sensors. (b) Dynamic step-response of the downstream sensor over time across discrete 100 sccm flow increments.

Figure 8 presents the experimental flow response at a constant 5 V heater input. At zero flow, both thermopile outputs were approximately 95.3 mV (Figure 8(a)). When the flow nitrogen is introduced, forced convection produces a net cooling effect, reducing the output voltages of both arrays. As the flow rate increased to 1100 sccm, the UP-TP signal decreases more rapidly than the DOWN-TP output voltage. Linear fits to the single-ended responses yielded absolute cooling sensitivities of 9.83 and 8.19 µV/sccm for UP-TP and DOWN-TP, respectively. At 1100 sccm, the corresponding outputs were 84.96 mV and 86.71 mV. The different cooling rates provide the differential signal. In Figure 8(b) successive 100 sccm increments produce distinct voltage steps and quasi-steady plateaus over the measurement interval.

The sensor was also tested in an anti-series configuration, in which the UP-TP and DOWN-TP thermopile chains were connected to measure the net differential Seebeck voltage directly. This configuration reduces the common-mode component and can improve rejection of disturbances that affect both thermopiles similarly, provided that the two channels remain thermally and electrically balanced.

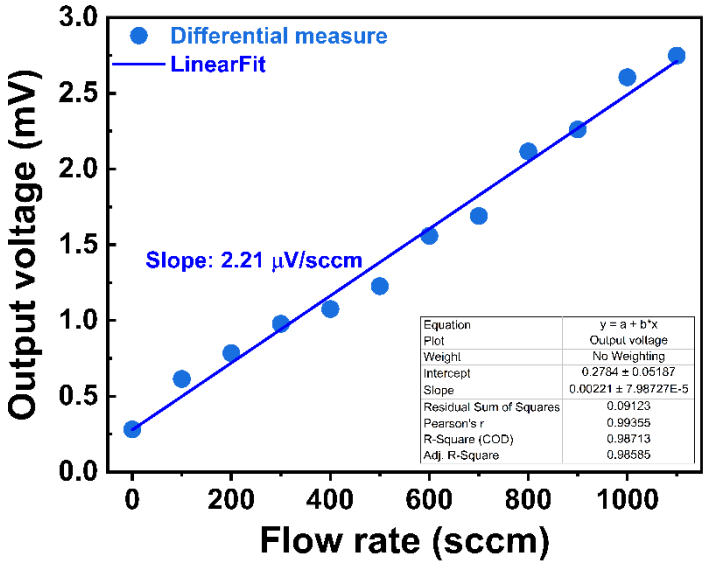
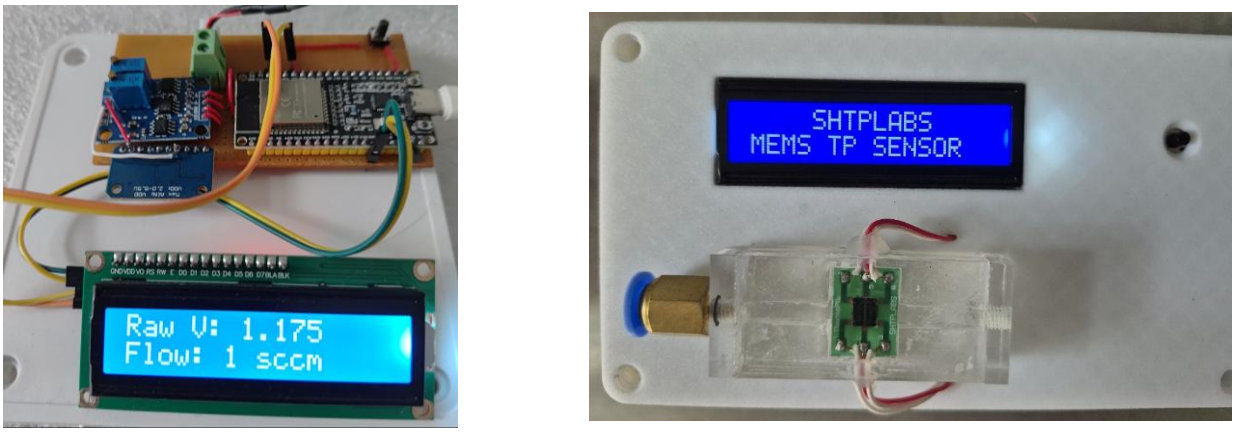


Figure 9: Experimental result for MEMS thermopile sensor showing the output voltage as a function of flow rate in the differential measurement.

Figure 9 presents the differential calorimetric response obtained from the anti-series configuration. The differential output increases approximately linearly from 0.28 mV at zero flow to about 2.7 mV at 1100 sccm. Linear regression over the 0-1100 sccm range yields a sensitivity of 2.21 ± 0.08 µV/sccm where the uncertainty is the standard error of the fitted slope. The nonzero intercept indicates a residual zero-flow offset.

4.4 Flow-meter prototype and system-level integration

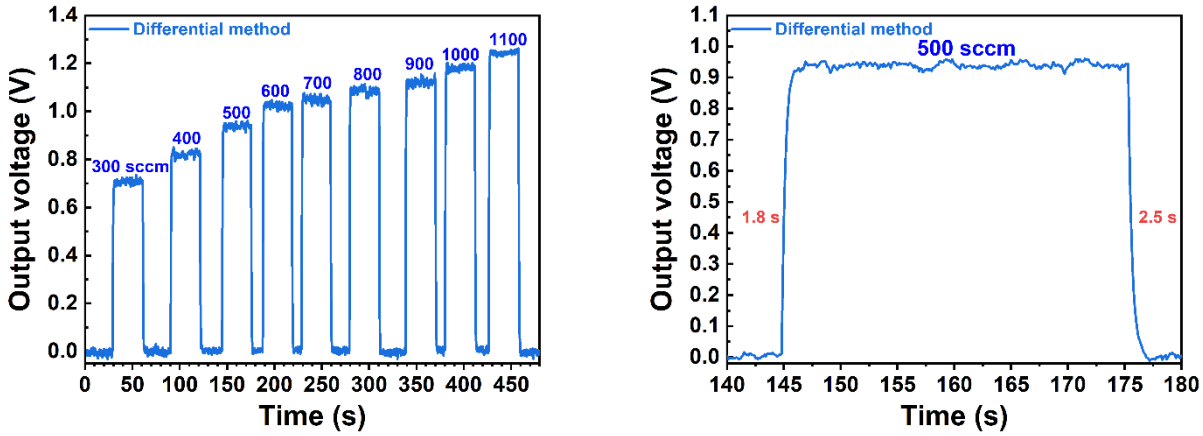
To demonstrate the practical applicability of the fabricated device, a standalone, real-time flow-metering prototype was developed based on the previously established differential measurement method. The integrated monitoring system comprises a packaged MEMS thermopile sensor interfaced with a custom signal-conditioning circuit. Because the raw differential Seebeck voltage is in the millivolt range, an AD620 instrumentation amplifier is used to amplify the signal. The amplifier circuit employs a 1 kΩ resistor in its gain-setting network, increasing the millivolt-level differential signal to a voltage range suitable for subsequent digitization. This amplified output is subsequently digitized by a high-precision ADS1115 analog-to-digital converter (ADC). An ESP32 NodeMCU (LuaNode32) microcontroller is utilized to process the digital data, applying the calibrated flow sensitivity to compute the actual gas flow rate. Finally, both the raw voltage and the calculated flow rate are continuously displayed on an I2C-integrated 1602 LCD module.



(a) (b)

Figure 10: Photographs of the continuous flow-monitoring prototype: (a) the internal electronic hardware for signal amplification and processing, and (b) the external view showing the packaged sensor and LCD readout.

This hardware integration in Figure 10 establishes a compact, highly responsive, and user-friendly platform, successfully validating the sensor's capability for continuous gaseous measurement in practical applications.



(a) (b)

Figure 11: System-level evaluation of the amplified flow-metering prototype: (a) Real-time dynamic step-response of the system under step-wise flow variations from 300 to 1100 sccm; and (b) Enlarged transient response of the differential flow-metering system at 500 sccm.

Following integration of the signal-conditioning circuitry, the millivolt-level differential Seebeck signal was amplified to approximately 0–1.25 V, providing a voltage range suitable for ADC digitization and subsequent processing. The real-time operational stability of the fully integrated flow-metering system is illustrated in Figure 11(a). When subjected to stepwise flow increments, the amplified output voltage showed distinct transitions and reached quasi-steady plateaus at each flow set point. Figure 11(b) shows that the differential thermopile flow sensor exhibits a response time of 1.8 s and a recovery time of 2.5 s at 500 sccm.

For system-level calibration, the packaged sensor was connected to an instrumentation amplifier, an ADC converter, and a processing unit. The amplified differential voltage was measured over the full flow range, including additional low-flow calibration points. Unlike the approximately linear direct sensor-output response obtained by multimeter measurement, the complete measurement chain exhibited a nonlinear voltage-flow relationship over the full range. A second-order polynomial was therefore fitted to the amplified voltage as a function of flow, and the inverse relation was implemented on the processing

unit to convert the digitized voltage into the displayed flow rate. The amplified voltage is the electrical output of the integrated measurement circuit, whereas the displayed value in sccm is calculated by the embedded calibration.

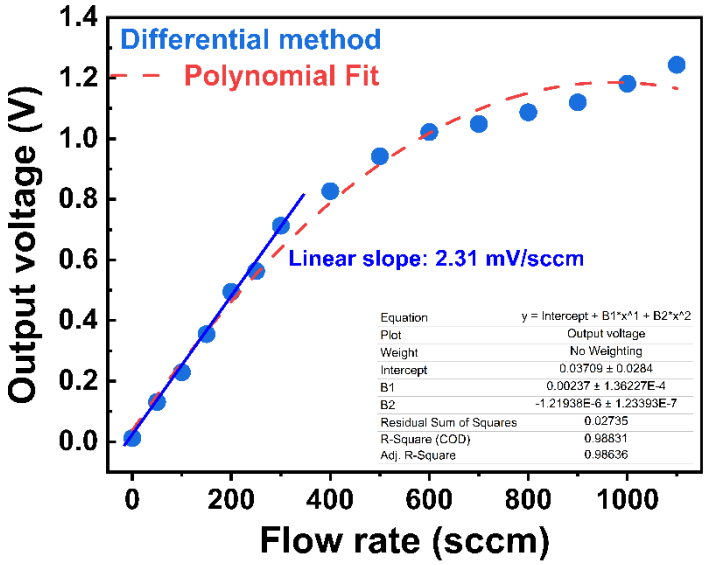


Figure 12: Amplified differential output voltage as a function of nitrogen flow rate. The response is approximately linear in the low-flow range (0-400 sccm), while a second-order polynomial fit describes the nonlinear response over the full 0–1100 sccm range.

As shown in Figure 12, the amplified differential output is approximately linear from 0 to 300 sccm, with a fitted slope of 2.31 mV/sccm. Over the full measurement range of 0-1100 sccm, however, the response becomes nonlinear and gradually approaches saturation as the nitrogen flow rate increases. This behavior is attributed to the diminishing change in convective heat transfer at higher flow rates, which causes the output curve to bend and plateau. Therefore, a second-order calibration curve was adopted rather than a purely linear model:

$$V_{amp} = 0.03709 + 0.00237Q - 1.21938 \times 10^{-6}Q^2 \quad (5)$$

where Q is the nitrogen flow rate in sccm, and V_{amp} is the amplified differential output voltage.

After polynomial calibration (Equation(5)) and implementation the inverse voltage-to-flow conversion on the ESP32, the system was evaluated using an independent measurement run. Table 1 compares the reference flow rate with the value displayed by the prototype. During validation, the measured data were transmitted through the USB interface and recorded on a connected computer.

Table 1: Independent validation of the calibrated flow-metering system by comparing the reference nitrogen flow rate with the system-displayed flow rate.

Reference flow rate (sccm)	Displayed flow rate (sccm)	Absolute error (sccm)	Relative error (%)
0	8	8	-
100	91	9	9.00%
200	209	9	4.50%
300	323	23	7.67%
400	423	23	5.75%
500	537	37	7.40%
600	642	42	7.00%
700	734	34	4.86%
800	792	8	1.00%
900	845	55	6.11%
1000	949	51	5.10%

Based on the independent validation dataset over the 0-1000 sccm range (11 points), the system achieved a mean-absolute-error MAE of 27.18 sccm and a root-mean-square-error RMSE of 32.00 sccm. The maximum absolute error was 55 sccm, corresponding to 5.50% of the 1000 sccm full-scale FS range, while the maximum relative error was 9.00%. During this validation, the system displayed a reading of 8 sccm at zero flow, indicating a residual zero-flow offset. To compensate for this residual offset, an automatic zero calibration is executed at startup under a confirmed no-flow condition. Additionally, the system is recalibrated at the zero-point whenever baseline drift is observed. In the repeatability tests described below, the zero calibration was applied, ensuring that all subsequent zero-flow measurements consistently registered as zero, as reflected in Table 2.

Table 2: Statistical evaluation of the repeatability and measurement stability of the calibrated flow-metering prototype over multiple measurement runs.

Reference flow rate (sccm)	Number of measurements	Mean displayed flow rate (sccm)	Standard deviation SD (sccm)	Coefficient of variation CV (%)
0	12	0	0	-
100	11	105	9.00	8.59%
200	14	194	15.7	8.08%
300	11	305	14.23	4.67%
400	14	408	23.99	5.87%
500	11	514	30.27	5.89%
600	14	601	31.55	5.25%
700	11	711	29.91	4.20%
800	14	799	33.01	4.13%
900	11	877	33.91	3.87%
1000	14	994	41.42	4.17%

The statistical results in Table 2 further demonstrate satisfactory repeatability across the repeated measurement runs. Excluding zero flow, the sample standard deviation (SD) ranges from 9.0 to 41.42 sccm, while the coefficient of variation (CV) remains between 3.87% and 8.59%. The highest relative variation occurs at 100 and 200 sccm, whereas the CV remains below 6% from 300 to 1000 sccm, indicating that the measurement dispersion is limited relative to the flow magnitude.

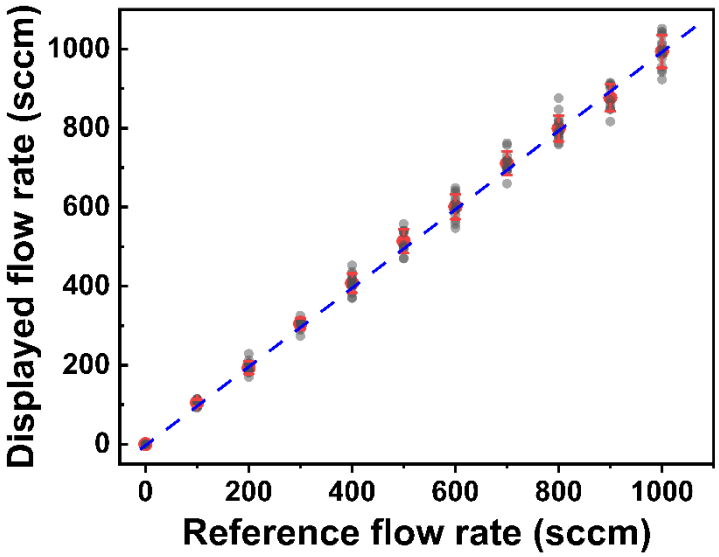


Figure 13: Repeatability and measurement stability of the calibrated flow-metering prototype over the 0–1000 sccm range.

Figure 13 summarize the repeatability and measurement stability of the calibrated flow-metering

prototype over the 0–1000 sccm range. The individual measurements are distributed around the ideal y = x line, while the mean displayed values remain close to the corresponding reference flow rates. Together with the statistical results in Table 2, these data indicate repeatable system-level performance under the tested conditions.

5 CONCLUSION

This work demonstrates the fabrication, characterization, and system-level integration of a Cr/Ni MEMS thermopile gas-flow sensor on a sub-20-μm suspended membrane. Backside DRIE produced a residual silicon membrane thickness of 17.57 ± 1.24 μm beneath an approximately 1.0 μm SiO_2 isolation layer. Each side of the central Ti/Ni microheater contains 20 series-connected Cr/Ni thermocouple pairs. Structural characterization by SEM, optical reflectometry, and surface profilometry confirmed the released membrane, oxide uniformity, and formation of the thermocouple junctions. Compared with the preceding thicker-membrane devices, the present structure produced substantially higher thermoelectric outputs under the same heater voltage and at comparable heater temperatures, demonstrating the improved thermal isolation achieved by reducing the suspended-membrane thickness.

The flow response was first characterized by direct multimeter measurement of the packaged sensor, before signal amplification and embedded conversion. At a 5 V heater input and over the 0–1100 sccm, the upstream and downstream thermopiles showed single-ended cooling sensitivities of 9.83 and 8.19 μV/sccm, respectively. An independent anti-series measurement yielded an approximately linear differential response with a sensitivity of 2.21 ± 0.08 μV/sccm. These measurements describe the direct electrical response of the packaged MEMS sensor.

The integrated prototype exhibited a response time of 1.8 s and a recovery time of 2.5 s. Independent validation of the displayed flow rate over 0-1000 sccm resulted in an MAE of 27.18 sccm, an RMSE of 32.00 sccm, a maximum full-scale error of 5.50%, and a maximum relative error of 9.00%. Across repeated measurement runs, the coefficient of variation ranged from 3.87% to 8.59%. The reported results are limited to nitrogen under the stated experimental conditions. Further work should address ambient-temperature compensation, denser low-flow calibration, quantified hysteresis and drift, extended-duration testing, verification of signal-chain linearity, and gas-specific calibration for gases with different thermal properties.

6 ACKNOWLEDGMENT

Saigon Hi-Tech Park financially supported this work under grant number: 96/2024/HĐ-QKHCN on Dec 23rd, 2024, and decision number: 1128/QĐ-SKHCN on Dec 18th, 2024. Xuan Thang Trinh was endorsed by the Faculty of Electrical Engineering Technology, Industrial University of Ho Chi Minh City, contract number: 51/HDGD (2026).

7 REFERENCES

[1] C. Il Hyun and K. D. Wise, A silicon-thermopile-based infrared sensing array for use in automated manufacturing, *IEEE Transactions on Electron Devices*, vol. 33, no. 1, pp. 72-79, 1986.

[2] A. W. Van Herwaarden and P. M. Sarro, Thermal sensors based on the Seebeck effect, *Sensors and Actuators*, vol. 10, no. 3, pp. 321-346, 1986.

[3] L. Jianguo, X. Bing, and L. Chenglu, Structure and properties of silicon-metal thermopile, *Sensors and Actuators A: Physical*, vol. 35, no. 3, pp. 217-220, 1993.

[4] N. T. Nguyen, Micromachined flow sensors—a review, *Flow Measurement and Instrumentation*, vol. 8, no. 1, pp. 7-16, 1997.

[5] L. C. Chang, Y. W. Deng, D. Lee, and C. S. Chen, Development of a High Resolution CMOS Flow Sensor, in *2006 1st IEEE International Conference on Nano/Micro Engineered and Molecular Systems*, pp. 890-895, 2006.

[6] S. Thapa, S. M. Tangutooru, E. J. Guilbeau, and N. D. Crews, The thermopile: An anisotropic temperature sensor, *Sensors and Actuators A: Physical*, vol. 187, pp. 132-140, 2012.

[7] D. Xu, Y. Wang, B. Xiong, and T. Li, MEMS-based thermoelectric infrared sensors: A review, *Frontiers of Mechanical Engineering*, vol. 12, no. 4, pp. 557-566, 2017.

[8] A. De Luca and F. Udrea, CMOS MEMS hot-film thermoelectronic flow sensor, *IEEE Sensors Letters*, vol. 1, no. 6, pp. 1-4, 2017.

[9] E. L. W. Gardner *et al.*, MEMS Thermal Flow Sensors— An Accuracy Investigation, *IEEE Sensors Journal*, vol. 19, no. 8, pp. 2991-2998, 2019.

[10] F. Ejeian *et al.*, Design and applications of MEMS flow sensors: A review, *Sensors and Actuators A: Physical*, vol. 295, pp. 483-502, 2019.
[11] H. Z. Ang Li, Yufei Zhou, Zhenjia Liu, A Review of CMOS-MEMS Thermal Flow Sensor, *Applied and Computational Engineering*, vol. 168, p. 11, 2025.
[12] K.-N. Lee, D.-S. Lee, S.-W. Jung, Y.-H. Jang, Y.-K. Kim, and W.-K. Seong, A high-temperature MEMS heater using suspended silicon structures, *Journal of Micromechanics and Microengineering*, vol. 19, no. 11, p. 115011, 2009/10/05 2009.
[13] W. Li, Z. Ni, J. Wang, and X. Li, A front-side microfabricated tiny-size thermopile infrared detector with high sensitivity and fast response, *IEEE Transactions on Electron Devices*, vol. 66, no. 5, pp. 2230-2237, 2019.
[14] Z. Liu *et al.*, A Thermopile-Based gas flow sensor with high sensitivity for noninvasive respiration monitoring, *Micromachines*, vol. 14, no. 5, p. 910, 2023.
[15] M. Li *et al.*, Fabrication and characterization of high-sensitivity, wide-range, and flexible MEMS thermal flow velocity sensors, *Microsystems & Nanoengineering*, vol. 10, no. 1, p. 102, 2024/07/22 2024.
[16] D. Yue *et al.*, A low-power, high-sensitivity CMOS-MEMS flow sensor for respiration health evaluation, *Chip*, vol. 5, no. 2, p. 100172, 2026/06/01/ 2026.
[17] N. Anh Tuan *et al.*, Design and performance analysis of a MEMS thermopile sensor for gas flow metering: Impact of membrane thickness, *TẠP CHÍ CÔNG THƯƠNG,* vol. 29, p. 8, 2025.

CHẾ TẠO, ĐÁNH GIÁ, VÀ TÍCH HỢP CẤP HỆ THỐNG CỦA CẢM BIẾN NHIỆT ĐIỆN Cr/Ni TRÊN MÀNG TREO DÀY DƯỚI 20-µm DÙNG CHO ĐO LƯU LƯỢNG KHÍ

NGUYỄN TUẤN ANH[1], HÀN PHÚ KHANG[2], NGUYỄN SĨ HOÀI VŨ[1], TRẦN DUY HOÀI[1], NGUYỄN THANH PHƯƠNG[1], ĐÀO MINH TUẤN[1], HUỲNH TRỌNG PHÁT[1], TRƯƠNG HỮU LÝ[1],NGUYỄN CHÍ CƯỜNG[3], TRỊNH XUÂN THẮNG[13]*

[1] Trung tâm Nghiên cứu Triển khai Khu Công nghệ cao, Việt Nam
[2] Khoa Khoa học Ứng dụng, Đại học Công nghệ Kỹ thuật Thành phố Hồ Chí Minh, Việt Nam
[3]Khoa Công nghệ Điện, Đại học Công nghiệp Thành phố Hồ Chí Minh, Việt Nam
** Tác giả liên hệ: thang_01038033@iuh.edu.vn*

Tóm tắt. Bài báo giới thiệu quá trình chế tạo, đánh giá đặc tính, và tích hợp cấp hệ thống của một cảm biến MEMS (hệ thống vi cơ điện) lưu lượng dòng khí được chế tạo trên màng treo dày dưới 20 µm. Thiết bị bao gồm một nguồn vi gia nhiệt Ti/Ni đặt tại trung tâm và hai chuỗi cặp nhiệt điện đối xứng, mỗi bên bao gồm 20 cặp nhiệt điện Cr/Ni mắc nối tiếp nhau, nằm trên một màng silicon dày 17,57 ± 1,24 µm cùng với lớp cách điện SiO2 dày khoảng 1,0 µm. Dựa trên việc tối ưu hóa độ dày màng từ nghiên cứu trước đó, báo cáo ghi nhận kết quả kích thước cấu trúc, đặc tính điện nhiệt, đo lưu lượng vi sai, xử lý tín hiệu và sự hiệu chuẩn thiết bị chế tạo. Trong điều kiện không có dòng khí, các dãy nhiệt điện phía trước và sau dòng thể hiện các tín hiệu phù hợp với đầu ra hiệu ứng Seebeck. Việc đánh giá đặc tính dòng khí nitơ N2 tại điện thế đầu vào 5 V nguồn gia nhiệt cho độ nhạy lần lượt là 9,83 và 8,19 µV/sccm trong các phép đo đơn tại đầu cuối làm mát; trong khi kỹ thuật kết nối ngược đầu độc lập cho độ nhạy vi sai là 2,21 ± 0,08 µV/sccm trong dải từ 0–1100 sccm. Cảm biến sau đó được tích hợp vào một nguyên mẫu đo lưu lượng độc lập đi kèm với mạch khuếch đại tín hiệu, bộ chuyển đổi tương tự - số và bộ xử lý vi điều khiển. Hàm đa thức bậc hai được sử dụng để hiệu chuẩn quy đổi phi tuyến toàn dải đo lưu lượng. Nguyên mẫu cho thấy thời gian đáp ứng và thời gian phục hồi lần lượt là 1,8 và 2,5 giây tại mức lưu lượng 500 sccm. Quá trình đo đạc độc lập trong dãy lưu lượng từ 0 đến1000 sccm xác định sai số tuyệt đối trung bình (MAE) là 27,18 sccm, sai số bình phương trung bình (RMSE) là 32,00 sccm và sai số toàn thang đo tối đa là 5,50%. Qua các lần đo lặp lại, hệ số biến thiên dao động từ 3,87% đến 8,59%. Những kết quả này minh chứng cho một nền tảng theo dõi lưu lượng khí nitơ nhỏ gọn, đồng thời, sự bù nhiệt độ môi trường và hiệu chuẩn theo từng loại khí là các yêu cầu cho quá trình phát triển tương lai.

Từ khóa: MEMS, cảm biến thermopile, cặp nhiệt điện Cr/Ni, màng treo, phép đo vi sai, mô hình đo lưu lượng, DRIE.

Received on August 26– 2026
Revised on October 08 – 2026